MIT Libraries | DSpace@MIT

MIT Open Access Articles

Critical role of IRF1 and BATF in forming chromatin landscape during type 1 regulatory cell differentiation

Massachusetts Institute of Technology

Critical role of the transcription factors IRF1 and BATF in preparing the chromatin landscape during Type 1 regulatory cell differentiation

Katarzyna Karwacz[1], **Emily R. Miraldi**[2,3], **Maria Pokrovskii**[3], **Asaf Madi**[1], **Nir Yosef**[4], **Ivo Wortman**[5], **Xi Chen**[6], **Aaron Watters**[2], **Nicholas Carriero**[2], **Amit Awashti**[7], **Aviv Regev**[5], **Richard Bonneau**[2,6], **Dan Littman**[3], and **Vijay K. Kuchroo**[1,*]

[1]Evergrande Center for Immunologic Diseases, Harvard Medical School and Brigham and Women's Hospital, Boston, MA 02115, USA

[2]Center for Computational Biology, Flatiron Institute, Simons Foundation New York, NY 10010, USA

[3]Skirball Institute for Biomolecular Medicine, NYU School of Medicine

[4]Department of Electrical Engineering and Computer Science and Center for Computational Biology, University of California, Berkeley, Berkeley, CA 94720, USA

[5]Broad Institute of MIT and Harvard, Cambridge, MA 02142, USA

[6]Department of Biology, New York University, New York, NY 10003, USA

[7]Center for Human Microbial Ecology, Translational Health Science and Technology Institute (an autonomous institute of Department of Biotechnology, Govt. of India), NCR Biotech Science Cluster, 3rd Milestone, Faridabad-Gurgaon Expressway, PO box # 4, Faridabad-121001, India

Abstract

Type 1 regulatory T (Tr1) cells are induced by interleukin-27 (IL-27) and have critical roles in the control of autoimmunity and resolution of inflammation. Here, we show that the transcription

*Corresponding author: Vijay Kuchroo (vkuchroo@evergrande.hms.harvard.edu).

factors IRF1 and BATF are induced early during treatment with IL-27 and are required for the differentiation and function of Tr1 cells *in vitro* and *in vivo*. Epigenetic and transcriptional analyses reveal that both transcription factors influence chromatin accessibility and expression of genes required for Tr1 cell function. IRF1 and BATF deficiencies uniquely alter the chromatin landscape, suggesting that these factors serve a pioneering function during Tr1 cell differentiation.

INTRODUCTION

IL-10-producing Type 1 regulatory T cells (Tr1 cells) were first described as a distinct subset of T cells induced *in vitro* by activating naive T cells in the presence of IL-10 [1]. They produce copious amounts of IL-10, their signature cytokine, but lack expression of Foxp3, the key transcription factor for differentiation of regulatory T (T_{reg}) cells. Tr1 cells' strong immunosuppressive capacity allows them to restrain autoimmune responses and alleviate pathology in models of autoimmune disease [2, 3, 4]. IL-27 suppresses Foxp3 expression but induces differentiation of Tr1 cells *in vitro* and *in vivo* [5, 6, 7]. *Il27ra*$^{-/-}$ mice lack Tr1 cells, have an increased number of T_H17 cells, both in the periphery and in the CNS, and, as a result, develop more severe EAE [8].

IL-27 receptor signaling induces expression of the transcription factor c-Maf, as well as the ligand-activated transcription factor aryl hydrocarbon receptor (AhR), which physically associate during Tr1 induction and together bind to and transactivate *Il10* and *Il21* promoters[9]. IL-21 acts as an autocrine growth factor for Tr1 cells [10]. IL-27 induces early growth response gene 2 (*Egr-2*) which controls Blimp1-mediated IL-10 upregulation through direct activation of the *Prdm1* promoter [11]. IL-27 thus induces transcription factors that regulate IL-10 production, but it is unclear whether it additionally regulates the chromatin landscape and access of transcription factors to key target genes.

During CD4$^+$ T cell differentiation, besides the "master regulator" transcription factors (TFs), a set of "pioneering factors" are induced that shape the epigenetic landscape in differentiating T cells, and regulate accessibility of transcriptional regulators to lineage specific genomic elements [12, 13, 14]. Recently, BATF and IRF4, were shown to regulate chromatin accessibility and exhibit pioneer-like functions during differentiation of T_H17 [15] and CD8$^+$ T cells [16]. Here we report that BATF and IRF1 are induced early during Tr1 differentiation and act as pioneering factors for differentiation of Tr1 cells.

RESULTS

IRF1 and BATF control Tr1 differentiation *in vitro*

We analyzed global gene expression following engagement of the TCR on naive CD4$^+$ T cells cultured in the presence (Tr1) or absence (T_H0) of IL-27. Analysis at 2 hours placed IRF1 and BATF amongst highly ranked putative transcription factors crucial for the regulation of Tr1 differentiation (Fig. 1a). Using qPCR, we found two waves of *Irf1* expression, peaking at around 3–6 hours and 12–15 hours after activation in the presence of IL-27, and two waves of *Batf* expression, peaking at roughly 1 and 24 hours (Fig. 1b). We activated naive CD4$^+$ T cells from *Irf1*$^{-/-}$ and *Batf*$^{-/-}$ mice in the presence of IL-27 and

analyzed T cell differentiation 72 hours later. Both $Irf1^{-/-}$ (Fig. 1c, d) and $Batf^{-/-}$ (Fig. 1e, f) cells failed to produce IL-10 (mRNA and protein), or differentiate into Tr1 cells and expressed decreased levels of interferon-γ (IFN-γ) (Fig. 1c, 1e).

Although there was a decrease in the percentage of total IFN-γ^+ cells and IFN-γ^+IL-10$^+$ cells in $Batf^{-/-}$ cells treated with IL-27, the frequency of IFN-γ^+IL-10$^-$ cells remained unchanged in the $Batf^{-/-}$ cells (Supplementary Fig. 1a). This may reflect the role of BATF in T_H1 cells, as IL-27 regulates T_H1 differentiation [17]. In contrast to Tr1 cells, we found enhanced differentiation of both $Irf1^{-/-}$ and $Batf^{-/-}$ cells into Foxp3$^+$ T$_{regs}$ (Supplementary Fig. 1b). Thus, IRF1 and BATF are indispensable for generation of IL-27 induced Tr1 cells *in vitro*.

The effects of IRF1 and BATF deficiency on Tr1 function

IL-27 treatment activates phosphorylation of STAT1 and STAT3, both of which are required for Tr1 differentiation [18]. We found that $Irf1$ expression was STAT1-dependent, but STAT3-independent (Fig. 2a). In contrast, $Batf$ expression was reduced in $Stat3^{-/-}$ cells, but remained unchanged in $Stat1^{-/-}$ cells (Fig. 2b).

Overexpression of IRF1, but not BATF, enhanced $Il10$ expression in IL-27-treated cells (Fig. 2c), although concurrent overexpression of IRF1 and BATF did not induce Il10 expression (Supplementary Fig. 1c). BATF overexpression strongly induced Maf and $Il21$ in Tr1 conditions, while both IRF1 and BATF augmented Ahr expression in cells treated with IL-27. These results point to separate roles played by IRF1 and BATF during Tr1 differentiation.

IRF1 affects induction and resolution of autoimmune disease

We induced EAE in $Irf1^{-/-}$ mice to assess the role of IRF1 in autoimmunity. In contrast to wild-type mice, in which clinical scores peak and diminish over time, $Irf1^{-/-}$ mice developed progressively more severe disease (Fig. 3a).

We found an increased percentage of IL-17A$^+$ and IFN-γ^+ CD4$^+$ T cells, with the most prominent change in the frequency of double cytokine-producing cells (IL-17A$^+$IFN-γ^+) in the CNS of $Irf1^{-/-}$ mice (Fig. 3b, 3c). Transfer of CD4$^+$ T cells from wildtype or $Irf1^{-/-}$ mice into $Rag2^{-/-}$ mice and induction of EAE in the recipients resulted in increased disease scores in recipients of the $Irf1^{-/-}$ CD4$^+$ T cells (Fig. 3d). Additionally, we crossed IRF1-deficient mice to TCR transgenic 2D2 mice[19] specific for MOG$_{35-55}$ ($Irf1^{-/-}$2D2). A small fraction (about 6%) of 2D2 transgenic mice generally develop spontaneous EAE; however, all $Irf1^{-/-}$ 2D2 mice developed spontaneous EAE (Fig. 3e), supporting a direct role for IRF1 in regulation of CD4$^+$ T cell responses in disease.

Proliferation of CD4$^+$ lymphocytes isolated from the spleen and draining lymph nodes of MOG$_{35-55}$ immunized $Irf1^{-/-}$ mice was strongly enhanced (Fig. 3f). Furthermore, these cells secreted more IL-17A and IFN-γ following restimulation with MOG$_{35-55}$ both in the presence or absence of IL-23 (Fig. 3g, h). Selected expression profiling of CD4$^+$ T cells (Supplementary Table 1) showed that in addition to $Il17$, $Irf1^{-/-}$ cells also upregulated $Rorc$,

Il23r, *Csf2*, *Runx3* and *Ifng* compared to wildtype controls when cells were restimulated in the presence of IL-23 (Supplementary Fig. 1d).

Batf^{−/−} mice are resistant to EAE [20] and *Batf*^{−/−} T cells failed to develop a T_H17 gene signature due to the requirement of BATF as a pioneering factor (Supplementary Fig. 1d). *Irf1*^{−/−} CD4^{+} T cells primed *in vitro* in T_H17 conditions produced increased levels of IL-17A (Supplementary Fig. 1e, f). Taken together, our results show that IRF1 deficiency promotes generation of Th17 cells *in vivo* and impairs resolution of autoimmunity in EAE.

IRF1 and BATF control generation of IL-10^{+} Tr1 cells *in vivo*

To determine whether IRF1 deficiency can affect IL-10 in lymphocytes during autoimmune inflammation, we induced EAE in wildtype and *Irf1*^{−/−} mice and isolated CD4^{+} T cells from the draining lymph nodes and the CNS at the beginning of the resolution of clinical disease (day 19). We found decreased amounts of *Il10* mRNA in both the CNS and the draining lymph nodes of *Irf1*^{−/−} animals (Fig. 4a).

We immunized wildtype mice with MOG_{35-55}, and analyzed CD4^{+} T cells reactivated *in vitro* in the presence of the MOG_{35-55} with or without IL-27. IL-27 induced 26 genes (>2-fold increase) and down-regulated 13 (>2-fold decrease), when compared to cultures activated without IL-27 (Fig. 4b), consistent with gene expression changes observed *in vitro* (Supplementary Fig. 1g). We compared the expression pattern of these 39 genes in T cells from immunized wildtype, *Irf1*^{−/−} and *Batf*^{−/−} mice re-stimulated in the presence of MOG_{35-55} and IL-27. Of these, *Il21*, *Il10*, *Prf1* and *Maf* were down-regulated in cells from both knockouts. Furthermore, *Irf1* and *Batf* deficient cells also differed from each other in their transcriptional responses (Fig. 4c).

We tested whether cells from *Irf1*^{−/−} and *Batf*^{−/−} mice can generate functional Tr1 cells. CD4^{+} T cells from immunized wildtype, *Irf1*^{−/−} and *Batf*^{−/−} animals were activated *in vitro* in the presence of IL-27 for three days and transferred into MOG_{35-55} immunized mice at the first clinical signs of disease (day 10). Transfer of wildtype Tr1 cells ameliorated disease, while transfer of Tr1-polarized *Batf*^{−/−} cells was ineffective in suppressing clinical disease, and transfer of IRF1-deficient Tr1 cells exacerbated disease (Fig. 4d). Consistent with these data, repeated administration of anti-CD3 antibody, which induces IL-10 in the mesenteric lymph nodes of wild-type C57/BL6 mice, failed to induce IL-10 in the *Irf1*^{−/−} or *Batf*^{−/−} mice (Fig. 4e). Furthermore, splenocytes from these mice failed to produce IL-10 upon restimulation (Fig. 4f). Thus, both IRF1 and BATF control generation of Tr1 cells *in vivo*.

IRF1 and BATF control the *Il10* locus

To test whether IRF1 and BATF can interact with the *Il10* promoter in CD4^{+} T cells, we differentiated wildtype naive CD4^{+} T cells for 72 hours in the presence of IL-27 and performed chromatin immunoprecipitation (ChIP), using antibodies against IRF1 and BATF, followed by qPCR. We used probes spanning previously described conserved non-coding sequences (CNS) and hypersensitivity (HSS) sites within the *Il10* locus [21, 22] (Fig. 5a). We detected IRF1 binding to the CNS-9, HSS-0.12 and HSS[+]2.98 sites (Fig. 5b), with HSS-0.12 containing two putative IRF1 binding sites [23] (designated later as HSS-0.12 site1 and site2). ChIP also revealed two BATF binding sites, at the CNS-9 and HSS[+]2.98 sites of the *Il10*

locus (Fig. 5c). As we observed some overlap between the IRF1 and BATF binding sites within the *Il10* locus, we tested the degree of co-occupancy of IRF1 and BATF using a sequential ChIP assay (ReChIP). We found a nearly complete (around 90%) co-occupancy of IRF1 and BATF at the CNS-9 site and a strong co-occupancy (around 60%) at the HSS⁺2.98 site (Fig. 5d). To evaluate a regulatory interaction between these two transcription factors, we performed ChIP for BATF in *Irf1⁻/⁻* and for IRF1 in *Batf⁻/⁻* Tr1 polarized cells. Binding of IRF1 and BATF in the *Il10* locus was markedly reduced in *Batf⁻/⁻* and *Irf1⁻/⁻* cells, respectively (Fig. 5e, f).

As BATF and IRF4 exhibit a similar dependency in T_H17 cells, we investigated potential competition for binding between IRF1 and IRF4 [24, 25]. Tr1 cells differentiated from *Irf4⁻/⁻* cells expressed increased IL-10 (Supplementary Fig. 2a), in contrast to *Irf1⁻/⁻* cells. Furthermore, overexpression of IRF1 antagonized IRF4-induced expression from an IL-17A reporter and IRF4 antagonized IRF1-induced expression from an IL-10 reporter in 293T cells (Supplementary Fig. 2b–2c and 2d–2e, respectively). We investigated binding of IRF1 to the IRF4 genomic binding sites on T_H17 associated (*Il17a, Il23r* and *Rorc*) loci, and found strongly increased IRF1 binding in IRF4-deficient T_H17 polarized cells (Supplementary Fig. 2f).

We analyzed whether IRF1 or BATF deficiency could affect distribution of epigenetic marks within the *Il10* locus in Tr1 polarized cells. We performed ChIP-qPCR assay in Tr1-primed cells with antibodies directed against H3K9Ac, H3K4me3 and H3K27me3. We found decreased recruitment of activating marks (H3K9Ac, H3K4me3) in the absence of both IRF1 and BATF, as well as increased repressive marks (H3K27me3) in cells from both knockouts (Fig. 5g). These results point to the role of both transcription factors in the induction of epigenetic changes during Tr1 differentiation, and possibly reveal one of the mechanisms by which IRF1 and BATF factors induce IL-10 following priming with IL-27.

Differential effects of IRF1 and BATF on the *Il10* promoter

To investigate whether IRF1 and BATF can directly transactivate the *Il10* promoter, we used reporter constructs driven by either the proximal *Il10* promoter (-1.5 kb) containing the HSS-0.12 site, or by the CNS-9 or HSS⁺2.98 regions cloned upstream of the *Il10* minimal promoter. C-Maf transactivation of the *Il10* proximal promoter was used as a control. IRF1 directly transactivated the *Il10* proximal promoter, while coexpression of IRF1 and c-Maf had an additive effect (Fig. 6a). Furthermore, IRF1 strongly transactivated expression regulated by the CNS-9 and HSS⁺2.98 regions of *Il10*, while BATF had no effect in transactivation of these constructs (Fig. 6b).

Overexpression of c-Maf in T_H0 cells induces IL-10 expression even without IL-27. We hypothesized that, in physiological conditions, this effect might depend on IRF1. We overexpressed c-Maf in wildtype and *Irf1⁻/⁻* CD4⁺ T cells; c-Maf was unable to fully induce IL-10 in *Irf1⁻/⁻* cells (Fig. 6c), indicating that c-Maf might not be able to bind to and/or transactivate the *Il10* locus in the absence of IRF1. Although BATF is required for c-Maf expression [26], overexpression of c-Maf failed to rescue the phenotype of *Batf⁻/⁻* cells polarized in Tr1 conditions. (Fig. 6d).

We then directly analyzed whether binding of c-Maf to the *Il10* locus is altered in *Irf1*^{−/−} cells. We performed ChIP with differentiated wildtype or *Irf1*^{−/−} Tr1-polarized cells and looked at known c-Maf binding sites within the *Il10* locus (MARE-1--4). We found that c-Maf binding was significantly reduced in *Irf1*^{−/−} cells (Fig. 6e).

In parallel, we analyzed whether BATF deficiency affected binding of other transcription factors known to bind to the *Il10* locus. As *Batf*^{−/−} cells do not express c-Maf, we investigated binding of AhR to the XRE1 site. We found that AhR fails to localize to its putative binding site in both *Irf1*^{−/−} and *Batf*^{−/−} Tr1 polarized cells (Fig. 6f). Collectively these results indicate that both IRF1 and BATF might induce chromatin changes that allow additional transcription factors to bind to and transactivate the *Il10* locus, suggesting a possible pioneer role in Tr1 cells for one or both of these factors.

BATF and IRF1 deficiencies alter the Tr1 chromatin landscape

To assess potential pioneering roles of BATF and IRF1 during Tr1 differentiation, we measured chromatin accessibility using ATAC-seq (Assay for transposase accessible chromatin using sequencing) in Tr1 cells deficient in BATF, IRF1, c-Maf and AhR, and compared each to the T_H0 and wildtype Tr1 controls. To capture chromatin landscape dynamics over the course of T-cell differentiation, we compared an early time point, 24h, which coincides with induction of *Il10* mRNA in cells treated with IL-27, and a late time point 72h. We detected ~180,000 accessible regions (peaks) across samples, and the data quality enabled quantitative analysis of peak intensities across sample conditions (Fig. 7a–c, Supplementary Fig. 3a). Time, polarization condition, and BATF deficiency most dramatically altered the chromatin landscape, with each perturbation leading to upwards of 20,000 altered accessible regions (FDR=10%, $\log_2$|fold-change|>1, Supplementary Fig. 3a).

To globally relate chromatin accessibility patterns across samples, we performed principal component analysis (PCA) (Supplementary Fig. 3b). At 24h, all samples displayed relatively similar chromatin landscapes, although small differences were seen between Tr1 and T_H0 polarizations for *Batf*^{−/−}, *Irf1*^{−/−}, and control cells. At 72h, the T_H0- vs. Tr1- dependent trends dominate; however the *Batf*^{−/−} chromatin landscape resembles neither Tr1 nor T_H0. At 72h (Fig. 7b), *Batf*^{−/−} T_H0 and Tr1 cells have a distinct chromatin accessibility pattern, whereas Tr1 cells derived from mice deficient in IRF1, AhR and c-Maf show relatively similar chromatin accessibility patterns. These analyses provide high-level support for BATF as a pioneering factor in Tr1 cells, consistent with its role in T_H17 and $CD8^+$ T cells[15, 16].

To address a potential pioneering role for IRF1, we performed differential analysis with DESeq2 to quantify the number of transcription factor-dependent accessible peaks per transcription factor in Tr1 conditions (Fig. 7c), subsampling to ensure equal statistical power for each knockout condition. In this controlled analysis, BATF deficiency led to altered accessibility ($\log2$(|fold-change|)>1, FDR = 10%) at over twenty thousand loci (ten thousand increased and ten thousand decreased). IRF1 deficiency resulted in ~100 peaks with increased accessibility and 1100 peaks with decreased accessibility. In contrast, AhR- and c-Maf-dependent alterations were minor, consistent with the heatmap in which BATF- and IRF1-dependent decreases in accessibility are apparent. Interestingly, each factor appears to affect unique regions. Additionally, BATF-dependent chromatin regions with increased

accessibility are visible in *Batf*^{−/−} *cells,* suggesting that, while much of the Tr1 landscape is being "turned off", new regions are also being "turned on".

Although the scale of IRF1- and BATF-dependent changes differs, both transcription factors alter chromatin accessibility, whereas c-Maf and AhR do not. This finding, combined with our data showing that both IRF1 and BATF are necessary for additional Tr1 transcription factors to bind chromatin, further supports a role for IRF1 and BATF as Tr1 pioneering factors. IRF1 is a smaller-scale/focused pioneer factor, while BATF acts globally.

BATF and IRF1 uniquely regulate Tr1 transcriptional programs

Although both *Irf1*^{−/−} and *Batf*^{−/−} cells fail to express IL-10 when stimulated with IL-27 *in vitro*, their unique chromatin accessibility patterns suggest the potential for divergent transcriptional programs. We treated wildtype, *Irf1*^{−/−} and *Batf*^{−/−} naive CD4^{+} T cells for 72 hours in Tr1 conditions and measured gene expression by RNA-seq. The Tr1 expression signatures were strikingly different among *Batf*^{−/−}, *Irf1*^{−/−}, and control cells (Supplementary Fig. 4a). In agreement with the ATAC-seq analysis, BATF deficiency led to the greatest number of differentially expressed genes (~500 genes, compared to ~110 for *Irf1*^{−/−}, Supplementary Fig. 4b, 4c). Deficiency of IRF1 and BATF resulted in large differences in transcription factor expression profiles (Fig. 7d), with down-regulation of the majority of transcription factors effected by BATF deficiency. Of these, only a few were also down-regulated in the IRF1-deficient cells and these shared transcription factors are reported to regulate IL-10 (e.g. *Hif1a* and *Prdm1*). Although *Rorc* is down-regulated in both IRF- and BATF-deficient cells, *Rora* is actually up-regulated in *Irf1*^{−/−} samples. Consistent with the loss of suppressive function in *Irf1*^{−/−} and *Batf*^{−/−} cells differentiated into Tr1 cells, reduced levels of cytokines associated with Tr1 functions, such as *Il10*, and of Perforin[2], were observed under both conditions (Fig. 7e)

We integrated the ATAC-seq and RNA-seq datasets to derive transcriptional regulatory networks for both IRF1- and BATF-deficient Tr1 cells. We integrated our quantitative ATAC-seq and RNA-seq information to find TFs that showed concurrent changes in expression and motif-containing peak accessibility. The relative perturbation strengths of IRF1 vs. BATF deficiencies are reflected in the scale of the resulting transcriptional regulatory networks. The changes induced by IRF1 deficiency are relatively limited (Fig. 7f, Supplementary Fig. 5). IRF1 putatively represses *Klf7*, as *Klf7* is over-expressed in *Irf1*^{−/−} cells and an accessible IRF1 motif is found *cis* to the Klf7 locus. The KLF7 motif, in turn, is enriched *cis* to genes with increased expression under IRF1-deficient conditions, such as *Id3* (Fig. 7g). STAT1 is also IRF1-dependent with an accessible IRF1 motif in *cis*, but STAT1 is a part of the Tr1 network that "turns off" in *Irf1*^{−/−} cells (*Ccl4, Il13ra1, Ccl3, Il10, Zbp1*) (Fig. 7g). IRF1 might also directly regulate expression of a number of genes, such as *Il10*, *Ccr5*, and *Prf1* (Fig. 7g).

The BATF Tr1 network is more complex, involving sixteen transcription factors (Fig. 7h,i). Explanations for the part of the Tr1 BATF network that is "turned on" can only be explained indirectly, by several transcription factors regulated downstream of BATF. The part of the Tr1 network that is "turned off" is explained not only by potentially direct BATF targets but also likely also involves secondary regulatory interactions, mediated by c-Maf, HIF1A,

FOSL2, ETS1, RUNX2, KLF10, RORG, RORA (Supplementary Fig. 6). BATF induces expression of *Klf10, Runx2, Prdm1, Hif1a, Fols2* and *Ets1,* whose expression is reduced in the *Batf*^{−/−} cells (Fig. 7i). They, in turn, might regulate a number of other cytokines or receptors that we found differentially expressed in the *Batf*^{−/−} T cells, such as *Il10, Prf1, Icos, Il2, Csf2, Cxcr5,* and *Il1rn.* The "off" network is connected to the "on" network by RUNX2 and KLF10, which putatively repress the "on" transcription factors *Eomes, Csr2, Sp6,* and several members of the NF-κB family. The *Batf*^{−/−} Tr1 transcriptional regulatory model suggests a dramatically altered transcriptional state for BATF-deficient Tr1 cells, mediated by several layers of altered transcriptional regulatory interactions.

DISCUSSION

Although IL-10 producing Foxp3^{−} Tr1 cells are critical for regulation of autoimmunity, Tr1 lineage defining factors or the pioneering factors that set up the genomic landscape for Tr1 differentiation were undefined. The greatest extent of transcriptome remodeling occurs during early phases of T cell activation, before lineage defining transcription factors are induced. To identify pioneering factors for Tr1 differentiation, we analyzed an early time point following IL-27 priming, to uncover the transcription factors that potentially establish a "Tr1 epigenetic landscape". IRF1 and BATF were strongly induced at 2 hrs following TCR activation and priming with IL-27. Both factors were indispensable for induction of Tr1 cells *in vitro* as well as for generation of Tr1 cells and protection from autoimmune disease *in vivo.*

During activation with IL-27, Tr1 cells activate both STAT-1 and STAT-3 to induce IL-10 production and develop a Tr1 transcriptional program. Previous studies have suggested that IL-27-induced STAT1 and STAT3 make distinct contributions to the transcriptional output. While STAT3 deficiency is associated with loss of the overall cytokine response, the major function of STAT1 is to provide specificity[27]. We found that IRF1 is expressed downstream of STAT1, while BATF expression is STAT3-dependent, which might account for some of the transcriptional differences observed between STAT1 and STAT3 deficiency.

Cooperative binding between BATF and IRF4 alters initial chromatin accessibility and thus pioneer access of transcription factors that specify the T_H17 developmental program[15]. AP-1 and IRF complexes also cooperatively promote transcription of the *Il10* gene in T_H17 cells[28]. IRF1 and BATF binding sites co-localized at two locations in the IL-10 promoter, and cooperative binding between them in Tr1 cells was supported by our findings that IRF1 and BATF occupancy in the *Il10* locus was markedly reduced in BATF- and IRF1-deficient cells, respectively.

Our results indicate that whereas BATF is required for the differentiation of both T_H17 and Tr1 cells, IRF4 and IRF1 are differentially required for the differentiation of these T cell subsets and therefore provide specificity in the regulation of the genomic landscape for T_H17 vs. Tr1 differentiation. Preferential binding of IRF1 to shared ISRE-sites would limit accessibility of IRF4 and inhibit T_H17 differentiation, whereas loss of IRF1 would inhibit Tr1 differentiation and promote unopposed binding of IRF4 and subsequent T_H17 differentiation, in agreement with our data. These opposing effects of IRF1 on Tr1 and T_H17

cell differentiation suggest that IRF1 might regulate balance between the two cell subsets and act as a molecular switch between the regulatory Tr1 cells and the pathogenic T_H17 cells. Consequently, both an increase in T_H17 cell differentiation and a decrease in Tr1 generation could contribute to the increased susceptibility to EAE in $Irf1^{-/-}$ mice.

Our data suggested that IRF1 and BATF must play a critical role in preparing the chromatin landscape for their binding and may serve as pioneer factors for the Tr1 lineage. Indeed our chromatin accessibility patterns data suggest that BATF and IRF1 prepare chromatin as crucial "early" mediators of IL-27-driven Tr1-specific transcription. Although smaller in scale than BATF deficiency, IRF1 deficiency altered a unique set of accessible regions and both TFs increased chromatin accessibility and facilitated binding of other transcription factors to the chromatin. Therefore, we propose that IRF1 is a "small-scale" pioneer factor affecting some chromatin regions that are indispensable for Tr1 differentiation. In contrast, BATF, which serves as a pioneer factor for a number of other cell types [15, 16], affected the chromatin landscape in undifferentiated T_H0 cells and had global effects on Tr1 differentiation. This suggests a general role for BATF as a pioneering factor for T helper cell differentiation. Integration of RNA-seq and ATAC-seq indicates that the BATF-dependent network consists of several layers of transcriptional interactions and that loss of BATF completely alters the IL-27-induced transcriptional state. Importantly, BATF appears to regulate *Il10* induction indirectly. The IRF1-dependent network is smaller, yet, IRF1 can regulate Tr1 differentiation both directly (through direct interaction of IRF1 with *Il10, Prf1*) and indirectly (through *Stat1* and *Klf7*).

Our studies have uncovered the critical role of two TFs, IRF1 and BATF, in preparing the chromatin landscape for induction of the Tr1 gene network in response to IL-27 signaling, where BATF acts as a pioneer factor and prepares the genomic landscape for the binding of additional transcription factors that define the Tr1 lineage. IRF1 specifically transactivates *Il10* gene expression and a smaller cluster of genes that characterize the Tr1 lineage, while restraining T_H17 differentiation. Together these data define BATF and IRF1 as drivers of the earliest steps in the induction of the Tr1 lineage.

MATERIALS AND METHODS

Animals

C57BL/6 (B6), B6.129S2-Irf1tm1Mak/J, B6.129S2-Batftm1.1mm/J and B6.SJL-PtprcaPepcb/BoyJ (CD45.1) were purchased from the Jackson Laboratories. B6.129S6-Rag2tm1Fwa N12, 129S6/SvEv-Stat1tm1Rds and 129S6/SvEvTac controls were purchased from Taconic. Animals were maintained in a conventional, pathogen-free facility at the Harvard Institutes of Medicine (Boston, MA) and all experiments were carried out in accordance with guidelines prescribed by the Institutional Animal Care and Use Committee (IACUC) at Harvard Medical School.

In vitro T cell isolation and differentiation

CD4$^+$ T cells from splenocytes and lymph nodes were isolated using CD4 microbeads (Miltenyi). Cells were further stained with antibodies against CD4, CD62L and CD44 and CD4$^+$CD62^{hi}CD44^{lo} naive cells were sorted by BD FacsAria (BD Biosciences).

Sorted cells were cultured in DMEM supplemented with 10% (vol/vol) FCS, 50 mM mercaptoethanol, 1 mM sodium pyruvate, nonessential amino acids, L-glutamine, and 100 U/ml penicillin and 100 g/ml streptomycin. For *in vitro* Tr1 differentiation, naive CD4$^+$CD62L^{hi}CD44^{lo} cells were sorted by flow cytometry and stimulated with plate bound anti-CD3 (145-2C11, 2 μg/ml) and anti-CD28 (PV-1, 2 μg/ml) in the presence of 25 ng/ml IL-27 (Ebioscience). IL-10 expression was assessed by flow cytometry 3 days later. For T$_H$17 differentiation, naive cells were stimulated in the presence of 20ng/ml rmIL-1β (Miltenyi Biotec), 25ng/ml rmIL-6 (Miltenyi Biotec) and rmIL-23 (R&D Biosystems). For T$_{reg}$ differentiation, naive cells were stimulated in the presence of 2.5ng/ml rhTGF-β1 (R&D Biosystems).

Flow cytometry staining and acquisition

Antibodies for flow cytometry were purchased from BioLegend and used as recommended by the manufacturer. For intracellular cytokine staining (ICS), cells were restimulated with PMA (Sigma, 50 ng/mL) and ionomycin (1 μg/ml, Sigma) and monensin (Golgistop; 1 μg/ml, BD Biosciences) for 4 hr. Following staining of surface markers, cells were fixed and permeabilized according to the manufacturer's instructions (BD biosciences). Cells were then analyzed on LSRII (BD Biosciences).

Measurement of cytokines

Secreted cytokines were measured after 72 hours of culture with ELISA.

Quantitative RT-PCR

RNA was extracted using RNAeasy microkit (Qiagen, USA), cDNA was prepared using iScript cDNA synthesis kit following the manufacturer's instructions (Bio-Rad, USA) and used as template for real-time PCR run on the ViiA 7 Real-Time PCR System (Applied Biosystems). Expression was normalized to *Gapdh*. The following primers-probes mixtures were purchased from Applied Biosystems: *Il10* (Mm01288386_m1), *Irf1* (Mm01288580_m1), *Batf* (Mm00479410_m1), *Il21* (Mm00517640_m1), *Maf* (Mm02581355_s1), *AhR* (Mm00478937_m1), *Gapdh* (Mm99999915_g1).

Chromatin immunoprecipitation (ChIP) and sequential ChIP (Re-ChIP)

Cells were polarized in Tr1 conditions for 3 days, fixed with 1% formaldehyde for 10 mins and quenched with 0.125M glycine. Chromatin fraction preparation and chromatin IP was performed using SimpleChIP Enzymatic Chromatin IP (Cell Signaling Technology) according to the manufacturer's instructions. The following antibodies were used: anti-IRF1 (Santa Cruz sc-640X), anti-BATF (Cell Signaling 8638S), anti-c-Maf (Santa Cruz sc-7866), anti-AhR (Enzo Life Sciences BML-SA210-0025), anti-trimethyl-Histone H3 (Lys4) (Millipore 07-473), anti-trimethyl-Histone H3 (Lys27) (Millipore 07-449), anti-Histone H3

(acetyl K9 (Abcam ab4441). For Re-ChIP, chromatin fraction was prepared as described above, and the chromatin IP was prepared using Re-ChIP-IT kit (Active Motif) according to manufacturer's instructions. ChIP and Re-ChIP quantitative PCR (qPCR) was run on Viia7 Real-Time PCR System (Applied Biosystems) and relative expression was calculated using Ct values of the samples and inputs. Primers spanning *Il17a* and *IL23r* sites were described before[29]. The following primer pairs were used for the rest of the targets:

CNS-20B fw: 5′-TTGGTATTCAGGGTGCTGTTC-3′,

CNS-20B rv: 5′-GTCCCTGAGGTGGAGGATAATA-3′,

CNS-9 fw: 5′-TTACAGAATGGCACTTCCAGAG-3′,

CNS-9 rv: 5′- CGATGTATTAGTTCCGGTGTGT-3′,

HSS-0.860 fw: 5′- ACCCAAACTGAGGTAGTAGGA-3′,

HSS-0.860 rv: 5′- AGCTGTTGAAGGATGGAGATG-3′,

HSS-0.610 fw: 5′- CCAAGGCTGGGACATTGTAA-3′,

HSS-0.610 rv: 5′- CCAGCATGAGAAGTTAGGAGAAG-3′,

HSS-2.0 fw: 5′- TCCTGAAACCCAGCTCAAATC-3′,

HSS-2.0 rv: 5′- CAAGTAAGGACCATGCAGAGAG-3′,

HSS-0.12 fw: 5′- TGAGTGCTAAGGTGACTTCC-3′,

HSS-0.12 rv: 5′- CGCACTCCCAGGTCATAAT-3′,

HSS^{+}0.92 fw: 5′- GTTGACACAGGTGCTCTTGA-3′,

HSS^{+}0.92 rv: 5′- CCTCTTGGGATCCAGTTGTTT-3′,

HSS^{+}1.65 fw: 5′- CCTTAGAGCCACCCAACAAATA-3′,

HSS^{+}1.65 rv: 5′- CAGAGACAGATGAGCAAGAGAC-3′,

HSS^{+}2.98 fw: 5′- GCGTCTCTGGCAGTTTCTAA-3′,

HSS^{+}2.98 rv: 5′- TCACTCTCCTCAACACCTAGT-3′,

HSS^{+}6.45 fw: 5′- ACACACACACACACACACA-3′,

HSS^{+}6.45 rv: 5′- CACTTCCTTCCGATGGTTACTT-3′

MARE-1 fw: GGAGAAAGTGAAAGGGATGGAG

MARE-1 rv: GGAATGGAATTGACTCAAGAACTG

MARE-2 fw: ACCCTCTACATGGGTCTACTT

MARE-2 rv: CAAGCAACTACTTGTCCTCCT

MARE-3 fw: AACTGAGTGCTAAGGTGACTTC

MARE-3 rv: TGGGCTATTCCAGAACATATTAGG

MARE-4 fw: TGCACTACCAAAGCCACAA

MARE-4 rv: GATCCTCATGCCAGTCAGTAAG

XRE-1 fw: CAGGTTGAGTGGAGGAAACAA

XRE-1 rv: CCCTCATCTGTGGATTCCATTC

Rorc1 fw: GCACAATGAGGGAACAGTAAGA

Rorc1 rv: CAGGAACTGGAGCCAATCAA

Rorc2 fw: TCACTCCTGCATCTTTCTCTTT

Rorc2 rv: TGCGATGGAACAGATTGAAGA

Luciferase assays

10^4 HEK293T cells were transfected with IL-10 firefly luciferase reporter constructs, renilla luciferase reporter and plasmids expressing IRF1, BATF, W11R[30] or c-Maf using Fugene. Cells were analyzed 48h later with the dual luciferase assay kit (New England Biolabs). Fragments containing the proximal *Il10* promoter (−1.5 kb including the HSS-0.12 site), and the CNS-9 or HSS+2.98 regions upstream of the *Il10* minimal promoter were described before [9, 31] and were cloned into pGL4.10 Luciferase reporter plasmid (Promega).

Retroviral infection

Naive CD4$^+$CD62L^{hi}CD44^{low} T cells were transduced with IRF1, BATF of c-Maf-expressing retroviruses as described previously[9] after activation with plate-bound anti-CD3 and anti-CD28 antibodies.

EAE induction, recall response and Tr1 transfer

For the induction of EAE, wildtype and *Irf1*$^{-/-}$ mice were immunized with 100μg of MOG$_{35-55}$ peptide (MEVGWYRSPFSRVVHLYRNGK) and 500μg of M. tuberculosis extract H37 Ra (Difco) emulsified in complete Freund's adjuvant (CFA). Mice were further injected intraperitoneally (i.p.) with 200ng pertussis toxin on days 0 and 2. Disease was scored daily on a scale of 0–5. For assessment of recall responses, mice were injected with 100μg MOG emulfisied in CFA. Spleens and lymph nodes were collected ten days later, and re-stimulated *in vitro* in the presence of MOG$_{35-55}$ (20μg/ml) and IL-23 or IL-27. Responses were assessed by flow cytometry, cytokine measurement and nanostring on CD4$^+$ sorted cells. For Tr1 transfer, wildtype, *Irf1*$^{-/-}$ and *Batf*$^{-/-}$ naive CD4$^+$ T cells were polarized for three days in Tr1 conditions and $3x10^6$ cells were transferred into wildtype mice immunized with MOG$_{35-55}$ 10 days after disease induction.

Isolation of cells from the CNS

Wildtype, *Irf1*$^{-/-}$ and *Batf*$^{-/-}$ mice were sacrificed at indicated time points and perfused with PBS. Brains and spinal cords were cut into small pieces and digested with Collagenase D (2.5 mg/ml; Roche) and Deoxyribonuclease I (1 mg/ml; Sigma-Aldrich) at 37°C for 20 minutes. Mononuclear cells were isolated over a 37%/70% Percoll gradient (GE Healthcare) and used for cytokine analysis with flow cytometry, or further sorted for CD45^{hi}CD3$^+$CD4$^+$ cells and used for qPCR.

NanoString gene expression analysis

Sorted CD4^{+} T cells were lysed using RLT buffer (Qiagen) and hybridized with a custom made CodeSet according to the manufacturer's instructions. Barcodes were counted (1,150 field of view sample) on an nCounter Digital Analyzer following manufacturer's protocol (NanoString Technologies Inc.). Data were analyzed using nSolver Analysis Software.

In vivo treatment with anti-CD3

Wildtype, *Irf1*^{−/−} or *Batf*^{−/−} mice were treated with 20μg of antibody targeted against CD3 (clone 2C11) or an isotype control administered i.p. every 3 days for a total of 3 times. Mice were sacrificed 4 hours after the last treatment. *Il10* expression in the mesentheric lymph nodes was analyzed by intracellular staining.

Statistical analysis

Statistical analysis was performed using Prism software (Graph Pad software, La Jolla, CA, USA). Linear regression with a 95% confidence interval, and unpaired, two-tailed Student's t-test were used for comparison of two groups. P values<0.05 were considered significant. ($P < 0.05 = *$; $P < 0.01 = **$; $P < 0.001 = ***$, $P < 0.0001 = ****$).

ATAC-seq

Samples were prepared as described previously[32]. Paired-end 50bp sequences were generated from samples on an Illumina HiSeq2500. Sequences were mapped to the murine genome (mm9) with bowtie2[33] (2.2.3), filtered based on mapping score (MAPQ >= 30, Samtools (0.1.19)), and duplicates removed (Picard). We then identify peak-centered, accessible regions across all samples. For each sample individually, we ran Peakdeck[34] (parameters –bin 75, -STEP 25, -back 10000, -npBack100000) and filtered peaks with a $P_{raw} < 1E-4$. We then limited accessible sequence to the region surrounding peak maxima, using a custom script to find peak maxima and Bedtools[35] (2.17.0) slop function to extend sequence by +/−25bp of the maxima. These peak-centric accessible regions were merged to generate a single reference peak annotation file, and reads per reference peak were counted with HTSeq-count[36]. This pipeline resulted in ~15 million reads per sample, ~30% of which mapped to the 180,478 identified peaks. We used DESeq2[37] to normalize and identify differentially accessible peaks across conditions. Downstream analysis and data visualization were performed in MATLAB R2014B.

RNA-seq

Samples were prepared as described previously[38] and sequenced on Illumina Hi-Seq 2500. Sequences were mapped to the murine genome (mm10) with STAR[39]. DESeq2 was used to normalize and identify differentially expressed transcripts across conditions. Downstream analysis and data visualization were performed in MATLAB R2014B.

Transcriptional regulatory networks

To define the Tr1 *Batf* KO and *Irf1* KO networks, we leveraged the quantitative nature of the ATAC-seq and RNA-seq datasets. Peaks were associated with putative transcription-factor (TF) binding events and target genes using a compendium of human and mouse TF motifs

downloaded from the ENCODE motif collection[40] (http://compbio.mit.edu/encode-motifs) and the CisBP motif collection[41] (http://cisbp.ccbr.utoronto.ca). Mouse motifs were also downloaded from the CisBP collection. We scanned peaks for individual motif occurrences with FIMO[42] (parameters --thresh .00001, --max-stored-scores 500000, and a first-order background model). In addition to leveraging motifs of human TF orthologs, we increased the mouse TF coverage of our motif database by additionally considering TF family subclasses[43]. We took advantage of similarities among TF subfamily sequence preferences to detect potential binding events of poorly characterized TF subfamily members. Putative binding events were associated with a target gene, if the peak fell within $^+$/−10kb of gene body. We used the KO RNA-seq datasets and defined potentially direct BATF or IRF1 regulatory interactions if (1) genes were differentially expressed (FDR=10% and had $\log_2|$fold-change$| >1$) and (2) the TF's motif occurred *cis* to the gene. To extend the networks, we defined sets of differentially expressed genes and tested (hypergeometric distribution, $P_{raw}<1E-3$) whether differentially expressed TFs had motifs enriched *cis* to a given set of genes, a procedure similar to Blatti et al[44]. In addition, we tested for enrichment limited to *cis* peaks having relevant patterns. For example, to define the BATF-dependent Tr1 network (e.g., the part of the network that turns "off"), we focused on the set of genes with decreased BATF-dependent expression, and searched for enrichment of TFs with decreased expression whose motif was either enriched *cis* when considering (1) all peaks or (2) only peaks that were decreased in accessibility (i.e., suggesting a concurrent decrease in binding event). For each KO Tr1 network, we looked for TF motif enrichment *cis* to genes increased (decreased) in expression and focusing on all peaks as well as those increased (decreased) in accessibility (suggesting activating interactions), and, to recover both activating and inhibitory interactions, we looked for enrichment *cis* to all differentially expressed genes. We used correlation between TF and target gene expression to infer interaction sign. Networks were visualized using a newly designed interactive interface[45], based on iPython[46] and packages: igraph[47], numpy and scipy[48]. The networks can be downloaded as tab-delimited text files, visualized in iPython notebooks and launched as binders from https://github.com/simonsfoundation/Tr1_batfKO.

Data availability

The data that support the findings of this study are available from the corresponding author upon request.

Supplementary Material

Refer to Web version on PubMed Central for supplementary material.

Acknowledgments

References

1. Roncarolo MG, et al. Interleukin-10-secreting type 1 regulatory T cells in rodents and humans. Immunol Rev. 2006; 212:28–50. [PubMed: 16903904]

2. Pot C, Apetoh L, Kuchroo VK. Type 1 regulatory T cells (Tr1) in autoimmunity. Seminars in immunology. 2011; 23:202–208. [PubMed: 21840222]

3. Astier AL, Meiffren G, Freeman S, Hafler DA. Alterations in CD46-mediated Tr1 regulatory T cells in patients with multiple sclerosis. J Clin Invest. 2006; 116:3252–3257. [PubMed: 17099776]

4. Barrat FJ, et al. In vitro generation of interleukin 10-producing regulatory CD4(+) T cells is induced by immunosuppressive drugs and inhibited by T helper type 1 (Th1)- and Th2-inducing cytokines. J Exp Med. 2002; 195:603–616. [PubMed: 11877483]

5. Awasthi A, et al. A dominant function for interleukin 27 in generating interleukin 10-producing anti-inflammatory T cells. Nature immunology. 2007; 8:1380–1389. [PubMed: 17994022]

6. Fitzgerald DC, et al. Suppressive effect of IL-27 on encephalitogenic Th17 cells and the effector phase of experimental autoimmune encephalomyelitis. Journal of immunology. 2007; 179:3268–3275.

7. Wang H, et al. IL-27 induces the differentiation of Tr1-like cells from human naive CD4+ T cells via the phosphorylation of STAT1 and STAT3. Immunology letters. 2011; 136:21–28. [PubMed: 21115047]

8. Batten M, et al. Interleukin 27 limits autoimmune encephalomyelitis by suppressing the development of interleukin 17-producing T cells. Nature immunology. 2006; 7:929–936. [PubMed: 16906167]

9. Apetoh L, et al. The aryl hydrocarbon receptor interacts with c-Maf to promote the differentiation of type 1 regulatory T cells induced by IL-27. Nature immunology. 2010; 11:854–861. [PubMed: 20676095]

10. Pot C, et al. Cutting edge: IL-27 induces the transcription factor c-Maf, cytokine IL-21, and the costimulatory receptor ICOS that coordinately act together to promote differentiation of IL-10-producing Tr1 cells. Journal of immunology. 2009; 183:797–801.

11. Iwasaki Y, et al. Egr-2 transcription factor is required for Blimp-1-mediated IL-10 production in IL-27-stimulated CD4+ T cells. European journal of immunology. 43:1063–1073.

12. Chang JT, Wherry EJ, Goldrath AW. Molecular regulation of effector and memory T cell differentiation. Nature immunology. 2014; 15:1104–1115. [PubMed: 25396352]

13. Josefowicz SZ. Regulators of chromatin state and transcription in CD4 T-cell polarization. Immunology. 2013; 139:299–308. [PubMed: 23590627]

14. Tripathi SK, Lahesmaa R. Transcriptional and epigenetic regulation of T-helper lineage specification. Immunological reviews. 2014; 261:62–83. [PubMed: 25123277]

15. Ciofani M, et al. A validated regulatory network for Th17 cell specification. Cell. 2012; 151:289–303. [PubMed: 23021777]

16. Kurachi M, et al. The transcription factor BATF operates as an essential differentiation checkpoint in early effector CD8+ T cells. Nature immunology. 2014; 15:373–383. [PubMed: 24584090]

17. Owaki T, et al. A role for IL-27 in early regulation of Th1 differentiation. Journal of immunology. 2005; 175:2191–2200.

18. Pot C, Apetoh L, Awasthi A, Kuchroo VK. Induction of regulatory Tr1 cells and inhibition of T(H)17 cells by IL-27. Seminars in immunology. 2011; 23:438–445. [PubMed: 21893418]

19. Bettelli E, et al. Myelin oligodendrocyte glycoprotein-specific T cell receptor transgenic mice develop spontaneous autoimmune optic neuritis. The Journal of experimental medicine. 2003; 197:1073–1081. [PubMed: 12732654]

20. Schraml BU, et al. The AP-1 transcription factor Batf controls T(H)17 differentiation. Nature. 2009; 460:405–409. [PubMed: 19578362]

21. Im SH, Hueber A, Monticelli S, Kang KH, Rao A. Chromatin-level regulation of the IL10 gene in T cells. J Biol Chem. 2004; 279:46818–46825. [PubMed: 15319439]

22. Jones EA, Flavell RA. Distal enhancer elements transcribe intergenic RNA in the IL-10 family gene cluster. J Immunol. 2005; 175:7437–7446. [PubMed: 16301651]

23. Mosser DM, Zhang X. Interleukin-10: new perspectives on an old cytokine. Immunological reviews. 2008; 226:205–218. [PubMed: 19161426]

24. Sjostrand M, et al. Expression of the immune regulator tripartite-motif 21 is controlled by IFN regulatory factors. Journal of immunology. 2013; 191:3753–3763.

25. Yoshida K, et al. Active repression of IFN regulatory factor-1-mediated transactivation by IFN regulatory factor-4. Int Immunol. 2005; 17:1463–1471. [PubMed: 16172134]

26. Ise W, et al. The transcription factor BATF controls the global regulators of class-switch recombination in both B cells and T cells. Nature immunology. 2011; 12:536–543. [PubMed: 21572431]

27. Hirahara K, et al. Asymmetric Action of STAT Transcription Factors Drives Transcriptional Outputs and Cytokine Specificity. Immunity. 2015; 42:877–889. [PubMed: 25992861]

28. Li P, et al. BATF-JUN is critical for IRF4-mediated transcription in T cells. Nature. 2012; 490:543–546. [PubMed: 22992523]

29. Glasmacher E, et al. A genomic regulatory element that directs assembly and function of immune-specific AP-1-IRF complexes. Science. 2012; 338:975–980. [PubMed: 22983707]

30. Eason DD, Shepherd AT, Blanck G. Interferon regulatory factor 1 tryptophan 11 to arginine point mutation abolishes DNA binding. Biochim Biophys Acta. 1999; 1446:140–144. [PubMed: 10395927]

31. Lee CG, et al. A distal cis-regulatory element, CNS-9, controls NFAT1 and IRF4-mediated IL-10 gene activation in T helper cells. Mol Immunol. 2009; 46:613–621. [PubMed: 18962896]

32. Buenrostro JD, Giresi PG, Zaba LC, Chang HY, Greenleaf WJ. Transposition of native chromatin for fast and sensitive epigenomic profiling of open chromatin, DNA-binding proteins and nucleosome position. Nat Methods. 2013; 10:1213–1218. [PubMed: 24097267]

33. Langmead B, Salzberg SL. Fast gapped-read alignment with Bowtie 2. Nat Methods. 2012; 9:357–359. [PubMed: 22388286]

34. McCarthy MT, O'Callaghan CA. PeaKDEck: a kernel density estimator-based peak calling program for DNaseI-seq data. Bioinformatics. 2014; 30:1302–1304. [PubMed: 24407222]

35. Quinlan AR, Hall IM. BEDTools: a flexible suite of utilities for comparing genomic features. Bioinformatics. 2010; 26:841–842. [PubMed: 20110278]

36. Anders S, Pyl PT, Huber W. HTSeq--a Python framework to work with high-throughput sequencing data. Bioinformatics. 2015; 31:166–169. [PubMed: 25260700]

37. Love MI, Huber W, Anders S. Moderated estimation of fold change and dispersion for RNA-seq data with DESeq2. Genome Biol. 2014; 15:550. [PubMed: 25516281]

38. Shishkin AA, et al. Simultaneous generation of many RNA-seq libraries in a single reaction. Nat Methods. 2015; 12:323–325. [PubMed: 25730492]

39. Dobin A, et al. STAR: ultrafast universal RNA-seq aligner. Bioinformatics. 2013; 29:15–21. [PubMed: 23104886]

40. Kheradpour P, Kellis M. Systematic discovery and characterization of regulatory motifs in ENCODE TF binding experiments. Nucleic Acids Res. 2014; 42:2976–2987. [PubMed: 24335146]

41. Weirauch MT, et al. Determination and inference of eukaryotic transcription factor sequence specificity. Cell. 2014; 158:1431–1443. [PubMed: 25215497]

42. Grant CE, Bailey TL, Noble WS. FIMO: scanning for occurrences of a given motif. Bioinformatics. 2011; 27:1017–1018. [PubMed: 21330290]

43. Wingender E, Schoeps T, Donitz J. TFClass: an expandable hierarchical classification of human transcription factors. Nucleic Acids Res. 2013; 41:D165–170. [PubMed: 23180794]

44. Blatti C, Kazemian M, Wolfe S, Brodsky M, Sinha S. Integrating motif, DNA accessibility and gene expression data to build regulatory maps in an organism. Nucleic Acids Res. 2015; 43:3998–4012. [PubMed: 25791631]

45. Watters AM, ER, Martins de Castro D, Pokrovskii M, Bonneau R. A fast-adapting, scriptable framework for gene regulatory network visualization. Submitted.

46. Pérez FG, BE. IPython: A System for Interactive Scientific Computing. Computing in Science & Engineering. Jun 18.2007 9:21–29.

47. Csardi GN, Tamas. The igraph software package for complex network research. InterJournal, Complex Systems. 2006:1–9.

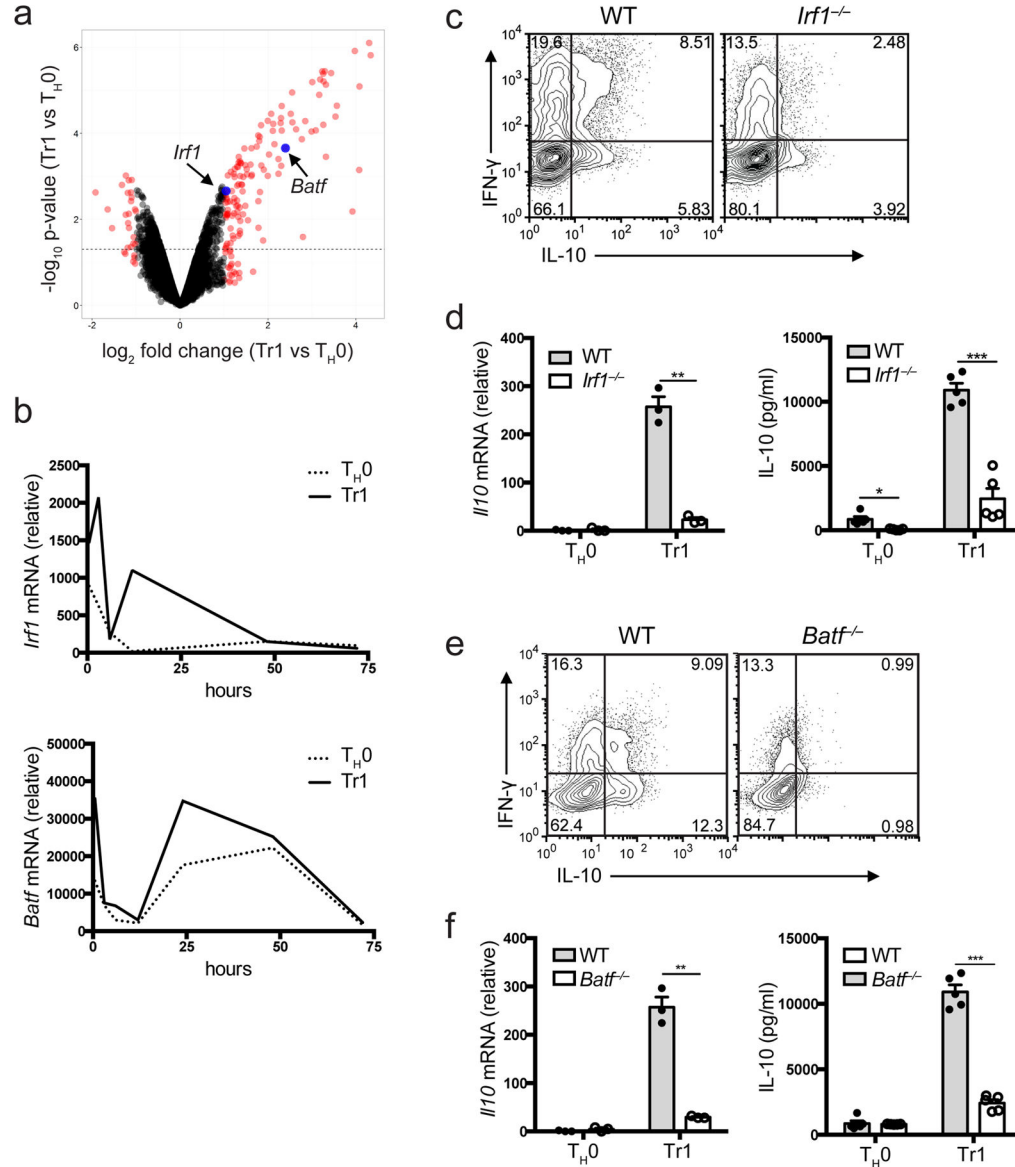48. Oliphant TE. Python for scientific computing. Computing in Science & Engineering. 2007; 9:10–20.

Figure 1. IRF1 and BATF are required for Tr1 differentiation *in vitro*

Naïve CD4^{+} T cells isolated from wildtype mice were primed with IL-27 in the presence of anti-CD3 and anti-CD28 antibodies **(a)** Volcano plot analysis for samples collected at 2 hours post cell stimulation. Depicted is time point of $\log_2$ fold-change (x-axis) versus $-\log_{10}$ p-value (y-axis, representing the probability that the gene is differentially expressed). Black dotted line marks p-value 0.05 and red dots marks fold change higher or lower than two. *Irf1* and *Batf* marked in blue. **(b)** *Irf1* and *Batf* mRNA expression measured by qPCR over 72 hours following cell stimulation. Analysis of Tr1 differentiation in *Irf1*^{−/−} cells 72 hours after cell priming with IL-27 measured by **(c)** flow cytometry **(d)** qPCR (left, n=3 samples) and ELISA (right, n=5 samples). Analysis of Tr1 differentiation in *Batf*^{−/−} cells 72 hours after cell priming with IL-27 measured by **(e)** flow cytometry **(f)** qPCR (left, n=3 samples) and ELISA (right, n=5 samples). Dots represent biological replicates. Data are representative

of three independent experiments (b), representative of four independent experiments (c, e), or are pooled from three independent experiments (d, f). *$P < 0.001$, **$P < 0.0001$ (unpaired t-test, error bars represent mean ±s.e.m.).
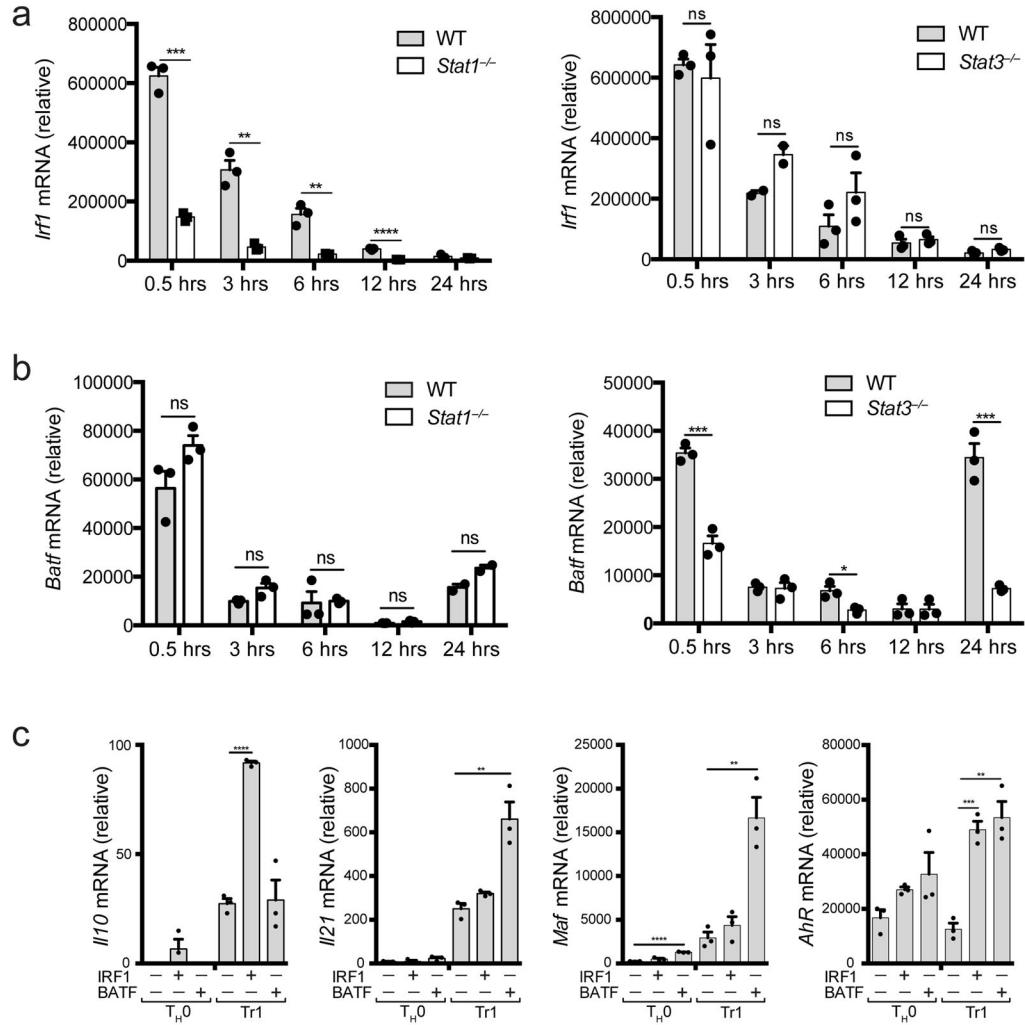
Figure 2. The effects of IRF1 and BATF deficiency on Tr1 function

(a) *Irf1* mRNA expression in *Stat1*$^{-/-}$ (left) and *Stat3*$^{-/-}$ (right) cells primed in the presence of IL-27. (b) *Batf* mRNA expression in *Stat1*$^{-/-}$ (left) and *Stat3*$^{-/-}$ (right) cells primed in the presence of IL-27. (c) Effects of IRF1 and BATF retroviral overexpression on *Il10*, *Il21*, *Maf* and *AhR* expression in cells treated in T_H0 or Tr1 conditions; mRNA levels were quantified using qPCR. Data are pooled from 3 independent experiments (a (*Stat1*$^{-/-}$), b, c; n=3 samples, dots represent biological replicates) or representative of 4 independent experiments (a (*Stat3*$^{-/-}$); n=3 samples, dots represent technical replicates). NS, not significant ($P>$ 0.05); *$P<$ 0.05, **$P<$ 0.01, ***$P<$ 0.001 and ****$P<$ 0.0001 (unpaired t-test, error bars represent mean ±s.e.m.).
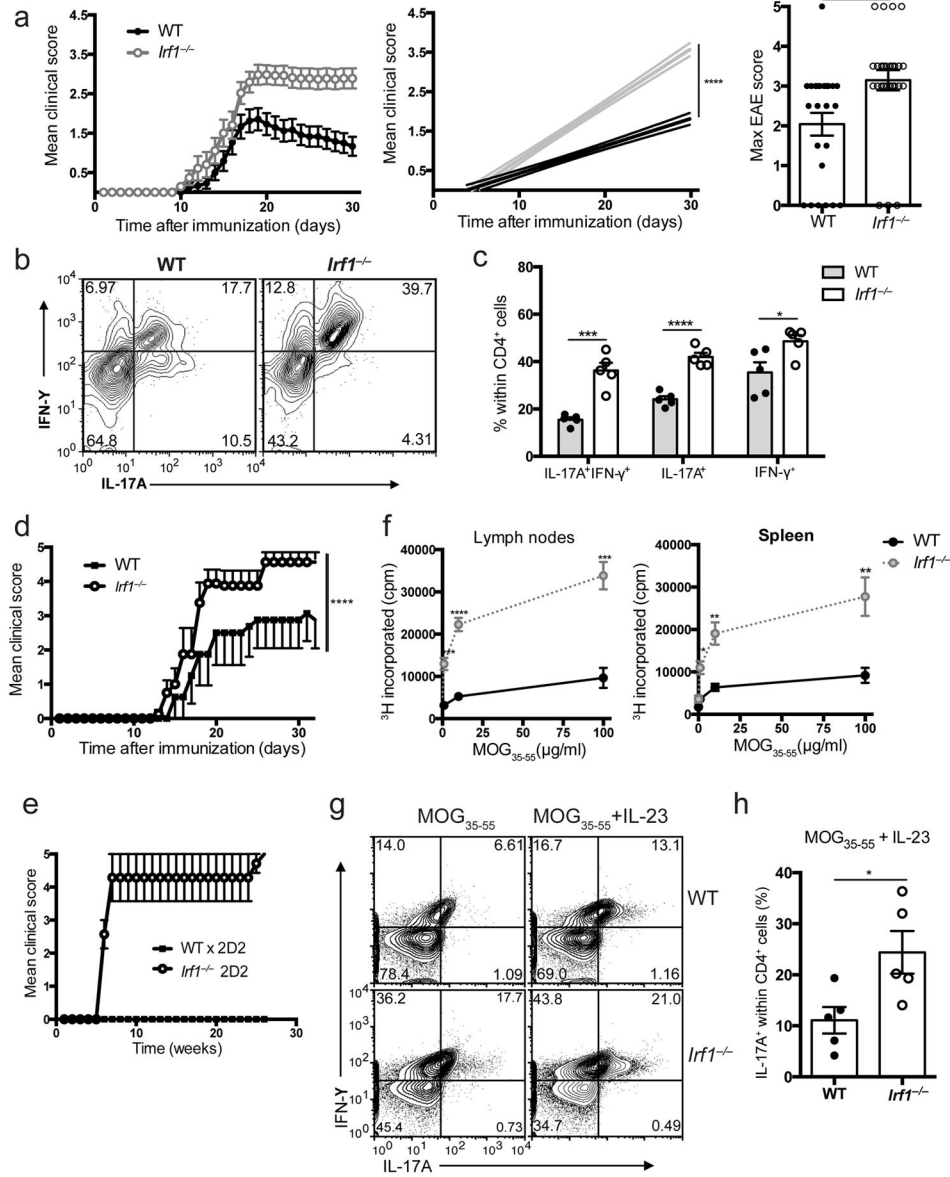
Figure 3. IRF1 affects induction and resolution of autoimmune disease
(a) EAE scores in WT and $Irf1^{-/-}$ mice were immunized with MOG_{35-55}, n=24 mice (WT) or n=27 mice ($Irf1^{-/-}$) (left); linear regression curve including the 95% confidence band of the regression line (middle); maximum scores (right). **(b)** Cytokine expression in $CD4^+$ T cells isolated from the CNS of WT and $Irf1^{-/-}$ mice at the peak of disease. **(c)** Frequency of $IL-17A^+$ and $IFN-\gamma^+$ cells within the $CD4^+$ T cells isolated from the CNS (n=5 mice). **(d)** EAE course in $Rag2^{-/-}$ mice with 2D2 or $Irf1^{-/-}$2D2 $CD4^+$ T cells transferred, followed by MOG_{35-55} immunization; n=8 mice/group. **(e)** Spontaneous EAE scores in 2D2 (n=5 mice) and $Irf1^{-/-}$ 2D2 mice (n=7 mice). **(f)** Spleens and lymph nodes from WT and $Irf1^{-/-}$ immunized mice were cultured with different concentration of MOG_{35-55}. ^3H thymidine was added to assess cell proliferation; n=5 samples. **(g)** Cytokine expression in $CD4^+$ T cells isolated from WT and $Irf1^{-/-}$ mice immunized with MOG_{35-55} and cultured with

MOG$_{35-55}$±IL23. **(h)** Quantification of (g); n=5 mice. Data are pooled from four independent experiments (a), representative of two independent experiments (b, f, g), or pooled from two independent experiments (c, d, h). Dots represent individual mice. *$P<$ 0.05, **$P<$ 0.01, ***$P<$ 0.001 and ****$P<$ 0.0001. Data represent mean ±s.e.m (linear regression (a (EAE plot), d; unpaired t-test (a (max score), c, f, h).

Figure 4. IRF1 and BATF control generation of IL-10+ Tr1 cells *in vivo*
(a) *Il10* expression in CD4+ T cells isolated from the CNS and dLNs (draining lymph nodes) of WT and *Irf1−/−* mice immunized with MOG35-55. Floating bars indicate min to max with a line at mean. **(b)** Gene expression fold change between CD4+ T cells isolated from wildtype mice immunized with MOG35-55 and re-stimulated in the presence of MOG35-55 ± IL-27. Genes with at least 2-fold change (MOG+IL-27/MOG) are shown. **(c)** Differential gene expression in WT, *Irf1−/−* and *Batf−/−* CD4+ T cells isolated from mice immunized with MOG35-55 and restimulated with MOG35-55 and IL-27. Gene-set created in (b) was used to generate the heatmap. **(d)** Tr1-polarized CD4+ T cells isolated from WT, *Irf1−/−* or *Batf−/−* mice were transferred into WT mice 10 days after EAE induction; n=7 mice (No Tr1, *Batf−/−*), n=8 (*Irf1−/−*), n=10 (WT Tr1). **(e)** IL-10 expression in mesenteric lymph nodes (MLN) from WT, *Irf1−/−* and *Batf−/−* mice injected with anti-CD3 antibody or an isotype control

(IC). **(f)** Splenocytes from mice in (e) were cultured for 72 hours, ELISA was used to measure IL-10 in the cultures. Dots represent individual mice. Data are pooled from three independent experiments (a), pooled from two independent experiments (b, c, d), representative of two independent experiments with n=3–4 mice pooled/group per experiment (e) or representative of two independent experiments (f). *$P < 0.05$, **$P < 0.01$ and ***$P < 0.0001$. Data represent mean ±s.e.m (unpaired t-test (a, f); linear regression analysis (d)).
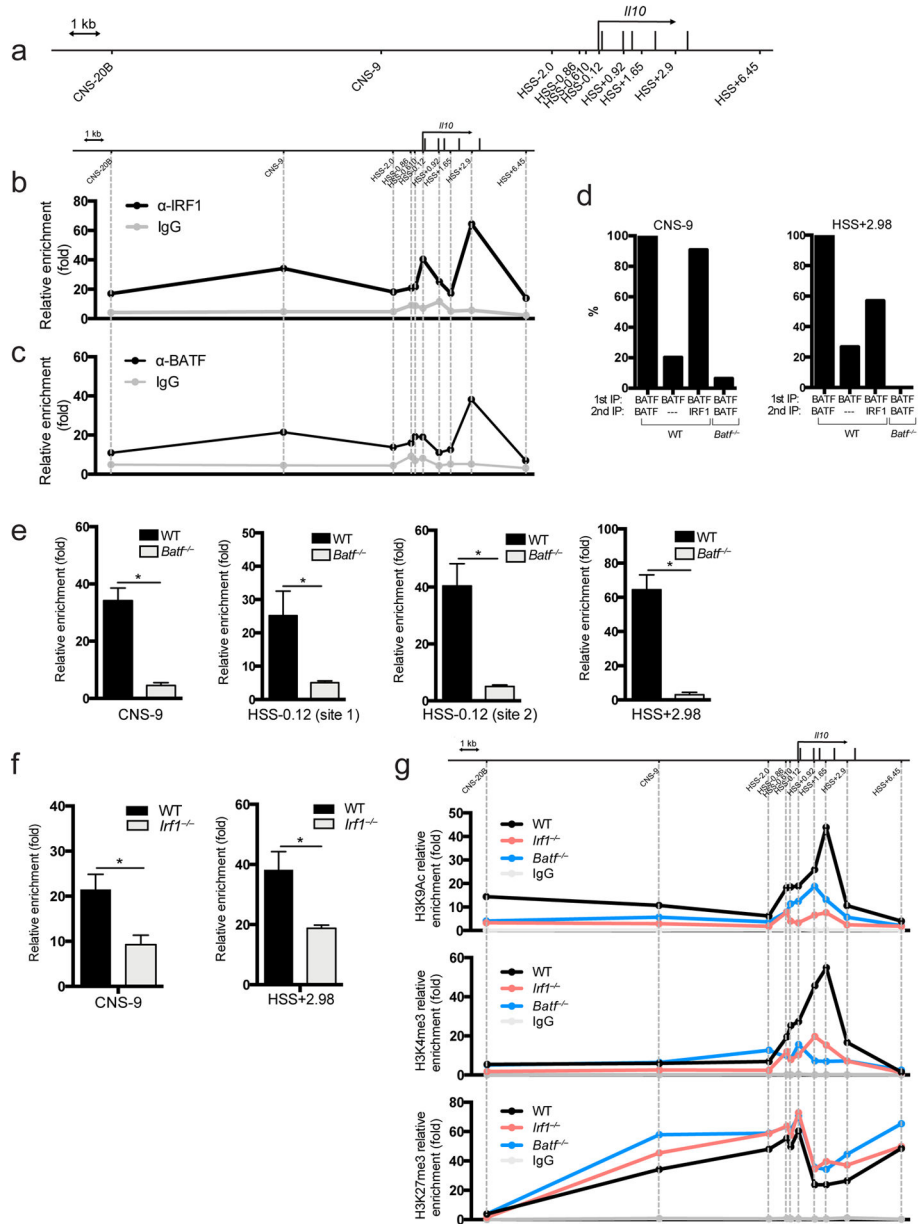
Figure 5. IRF1 and BATF bind to the *Il10* locus
(**a**) Schematic drawing of the *Il10* locus; known CNS and HSS sites are marked. ChIP analysis of (**b**) IRF1 (n=2 samples) and (**c**) BATF (n=3 samples) interactions within the *Il10* promoter in WT Tr1 cells polarized for 72 hrs. (**d**) Sequential ChIP analysis of BATF and IRF1 interactions in the CNS-9 and HSS+2.98 regions of the *Il10* promoter in WT and *Batf* −/− cells differentiated in the presence of IL-27. (**e**) ChIP analysis of IRF1 binding in the CNS-9, HSS-0.12, HSS+2.98 sites of the *Il10* promoter in WT and *Batf*−/− cells differentiated in Tr1 conditions; n=2 samples. (**f**) ChIP analysis of BATF binding in the CNS-9, and HSS+2.98 sites of the *Il10* promoter in WT and *Irf1*−/− cells differentiated in Tr1 conditions; n=3 samples. (**g**) ChIP analysis of epigenetic marks recruitment to the *Il10* promoter in WT, *Irf1*−/− and *Batf*−/− cells differentiated in Tr1 conditions. Data are

representative of three independent experiments with similar results (b, c, e, f) or two independent experiments (d, g). *$P < 0.05$ (unpaired t-test, error bars represent mean ±s.e.m.).
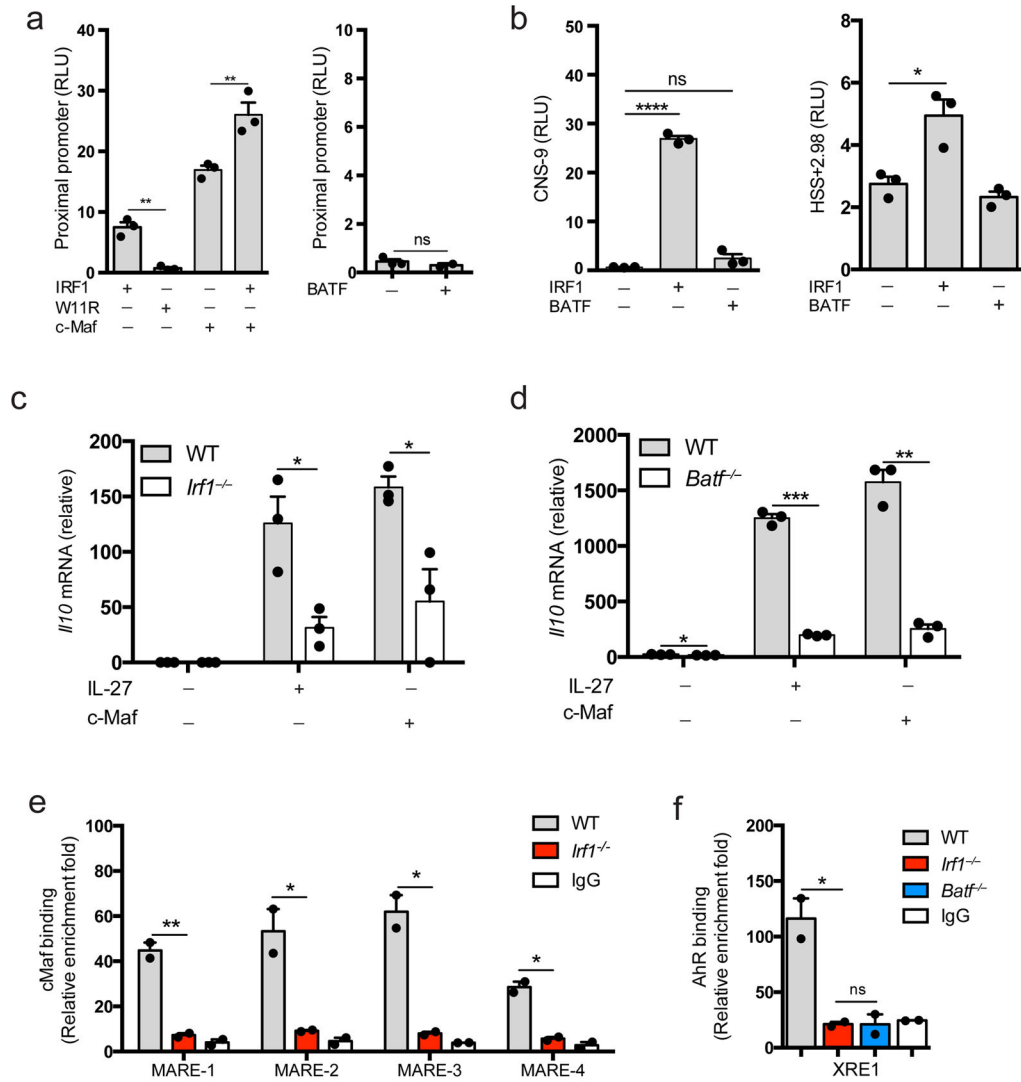
Figure 6. IRF1 and BATF control the *Il10* locus
Luciferase activity in 293T cells transfected with different IL-10 luciferase reporters in the presence of constructs encoding IRF1, IRF1 DNA-binding mutant W11R, c-Maf and BATF. RLU (Relative Light Units) are shown. **(a)** Proximal promoter indicates the proximal 1.5 kb region of the promoter. **(b)** CNS-9 and HSS[+]2.98 reporters contain the *Il10* promoter fragments cloned upstream of the *Il10* minimal promoter. **(c)** *Il10* expression (mRNA) in WT and *Irf1*^{−/−} CD4^{+} T cells retrovirally transduced with c-Maf and cultured in T_H0 or Tr1 conditions **(d)** *Il10* expression (mRNA) in WT and *Batf*^{−/−} CD4^{+} T cells retrovirally transduced with c-Maf and cultured in T_H0 or Tr1 conditions **(e)** ChIP analysis of c-Maf interactions with c-Maf-binding sites (MARE-1--4) in the *Il10* promoter in WT and *Irf1*^{−/−} Tr1 polarized cells. **(f)** ChIP analysis of AhR interactions with AhR-binding site XRE-1 in the *Il10* promoter in WT, *Irf1*^{−/−} and *Batf*^{−/−} Tr1 polarized cells. Data are representative of three independent experiments (a, b; n=3 samples), representative of two independent experiments (c, d; n=3 samples) or pooled from two independent experiments (e, f). Dots

represent technical replicates (a, b, c, d) or biological replicates (e, f). NS, not significant ($P > 0.05$); $*P < 0.05$, $**P < 0.01$, $***P < 0.001$ and $****P < 0.0001$.
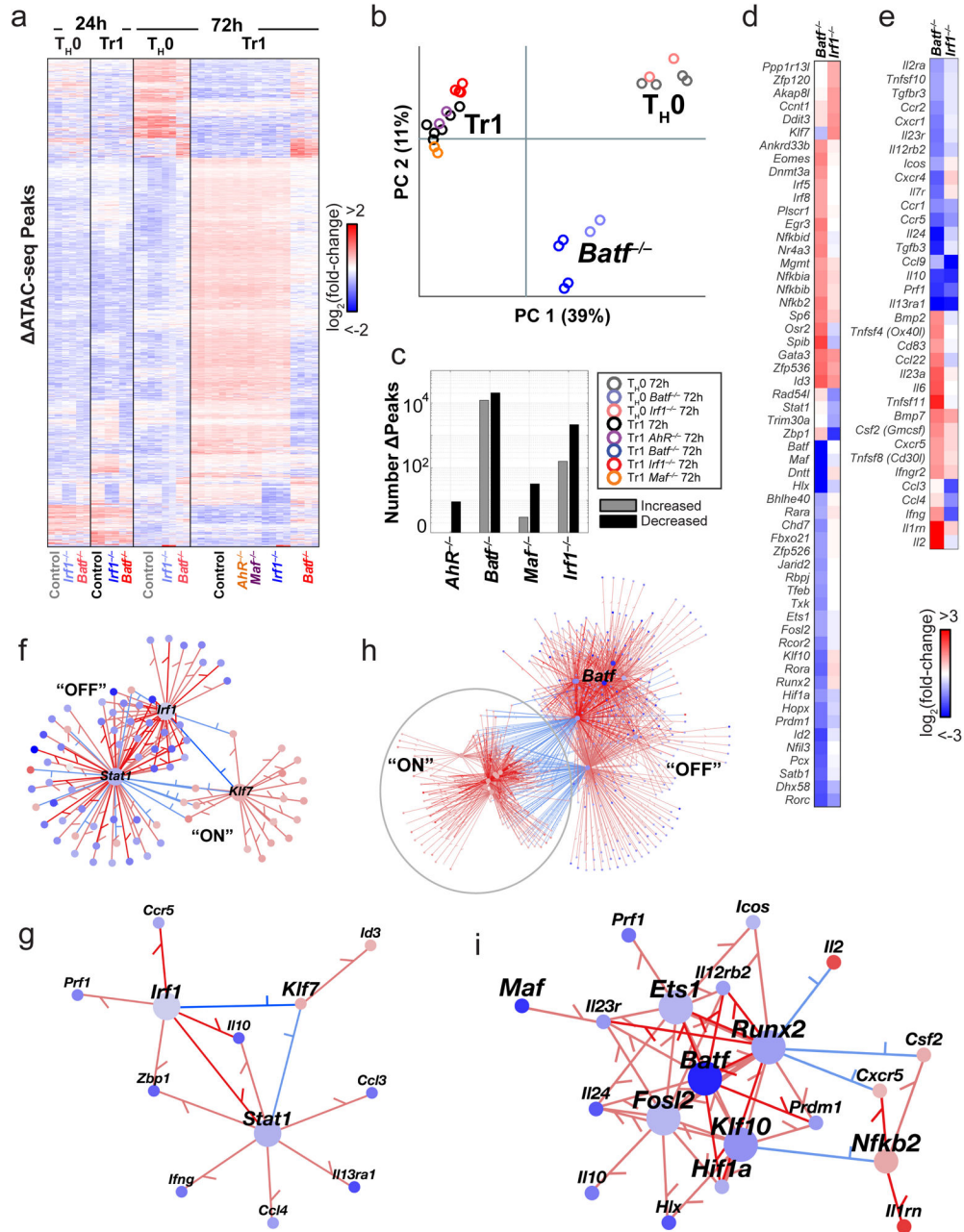
Fig 7. BATF- and IRF1-deficiences uniquely contribute to Tr1 chromatin and transcriptional landscapes

(a) Heatmap of normalized ATAC-seq peak intensities (log$_2$-fold-changes relative to the mean for each peak). Limited to (6017) peaks that are condition-dependent with log$_2$|FC|>3 and FDR=1% for at least one pairwise comparison of interest. (b) PCA of the 72h conditions, using all ATAC-seq peaks in the dataset (180,478 DESeq2-normalized peak intensities). (c) Number of differentially accessible peaks detected using DESeq2, comparing Tr1 KO (knockouts) to control cells at 72h, log$_2$|FC|>1 and FDR=10% (Subsampled, each comparison had n=2 (KO), n=6 (control)). Estimates of log$_2$-fold-changes in gene expression from RNA-seq data, comparing either *Batf*$^{-/-}$ or *Irf1*$^{-/-}$ and

control Tr1 cells ($\log_2$|FC|>1, FDR=10%) for DNA-binding proteins **(d)** and cytokines and cytokine receptors **(e)**. RNA-seq and ATAC-seq datasets were integrated to generate putative transcriptional regulatory networks for *Irf1*$^{-/-}$ **(f–g)** and *Batf*$^{-/-}$ **(h–i)** Tr1 cells. Nodes represent differentially expressed transcription factors and target genes, colored according to relative gene expression ($\log_2$(KO/Control)) at 72h; red and blue indicate high and low relative expression, respectively. Edges are drawn between TFs and putative gene targets if that differentially expressed TF's motif was enriched in ATAC-seq peaks *cis* to genes that were increased or decreased in response to KO ($P_{raw}<10^{-3}$, hypergeometric CDF). Edge colors (blue - inhibitory, red - activating) are based on correlation between TF and putative target gene expression. "ON" indicates genes de-repressed in the knockout cells, while "OFF" indicates genes repressed in the knockout cells.